Journal of
Nanotechnology and Smart Materials

JScholar
Fostering Scholarly Communication

Research Article Open Access

Tuning Nonlinear Optical Properties in Single Lens-Shaped Core/Shell Under Combined Effects of Temperature, Pressure, Transverse Electric and Magnetic Fields

M Choubani*, H Maaref and F Saidi

Laboratoire de Micro-Optoélectronique et Nanostructure (LR99ES29), Departement of Physique, Faculty of Sciences Monastir, University of Monastir, Tunisia

***Corresponding author:** M Choubani, Laboratoire de Micro-Optoélectronique et Nanostructure (LR99ES29), Departement of Physique, Faculty of Sciences, Monastir, University of Monastir, Tunisia, Tel: +216 27785483, E-mail: mohsenchoubani3@yahoo.fr

Received Date: October 28, 2021 **Accepted Date:** November 28, 2021 **Published Date:** November 30, 2021

Citation: M Choubani (2021) Tuning Nonlinear Optical Properties in Single Lens-Shaped Core/Shell Under Combined Effects of Temperature, Pressure, Transverse Electric and Magnetic Fields. J Nanotech Smart Mater 7: 1-14.

Abstract

In this paper, we have interested in the optimization of the nonlinear optical rectification (NOR) and the intra-band transition lifetime (τ) of carriers in single lens-shaped InAs/GaAs core/shell. The energy levels and the envelope wave functions are calculated by using the Finite Difference Method (FDM) and within the framework of the effective mass- approximation. The obtained results clearly showed that the structure dimensions, the wetting layer (WL), the pressure (P), the temperature (T), the electric (F) and the magnetic (B) fields dramatically affected τ, NOR magnitude and the attributed resonant energy (ω_{res}). Besides, the resonant energy can be blue or red-shifted energies, depending on the proofs revealed above. Moreover, obtained results showed that the NOR achieved and optimum magnitude when the transverse electric field was applied along one side of the cross-section of the structure under investigation. Also, the opposite effects caused by hydrostatic pressure and temperature reveal a big practical interest and offer an alternative way to tuning of the NOR in optoelectronic devices.

Keywords: Electromagnetic fields; Lens-shaped core/shell; Nonlinear Optical Rectification; Pressure' Temperature' Transition lifetime

Introduction

Semiconductor nanostructures, known as quantum dots (QDs), have recently attracted a great attention for application in various fields such as photo-detectors [1], QD- based lasers [2] and solar cells [3]. So, a number of efforts have been expended on InAs QDs embedded in GaAs matrix. Such structures can be obtained by using the Stranski- Krastanov (SK) technique [4]. During the epitaxial method, when the active layer (InAs) reaches to a critical thickness about 0.5 nm ≈ 1.7 mono- **layer [5],** so-called wetting layer (WL), accumulated strain energy forces transition from two-dimensional (2D) growing to 3D islands. This is due to the lattice mismatching between InAs and GaAs materials, which is about 7%. Many experimental studies have revealed that the unavoidable effect of the WL on the electronic and optical properties of semiconductor QDs systems is of significant importance [6]. However, in many theoretical works, the WL effect has been neglected for sake of simplicity [7,8] to solve the three-dimensional (3D) Schrödinger equation. To present a precise study, one should consider QD coupled to its WL. Also, electronic and optical properties of these nanostructures such as transition energies, transition dipole moment and oscillator strength are strongly size dependent and sensitive to height and base length of these QDs [9,10].

According to the literature, different shapes of QDs, such as elliptical- shaped [11], spherical- shaped [12], cylindrical- shaped [13] and pyramidal- shaped [14] have been investigated over the years to describe the 3D confinement in InAs/GaAs systems. However, from the Atomic Force Microscopy (AFM) and Electronic Transmission Microscopy (TEM) results, it is found that the lens- shape is the most realistic model of the QD [15, 16]. Recently, more attention has been focused on the study of core/shell nanostructures because of their importance in the electric and optical properties. So, more phenomena can be clearly shown [17-21]. In many recent works, we have presumed that the Nonlinear Optical Properties (NLOP) related to intra-band transitions are greatly enhanced in core/shell systems in both theoretical and experimental sides. Among, the nonlinear optical properties: the Second Harmonic Generation (SHG), the Nonlinear Optical Rectification (NOR), linear, nonlinear and total optical absorption coefficients. However, we have perceived that particular modulated shapes are considered with and without the wetting layer effect. Also, combined effects of the hydrostatic pressure and the temperature on the mentioned nonlinear optical properties are not introduced together. Moreover, the transition lifetime of carriers in core/shell structures has not been also studied extensively in the literature. Likewise, the effective- mass and the confining potential of carriers are considered constant. However, the confining potential and the electron effective- mass are temperature and pressure dependent quantities. In the present work, we search to optimize the NOR coefficient in lens-shaped InAs/GaAs core/shell with taking into account the wetting layer effect (WL), the hydrostatic pressure (P) and the temperature (T) effects. The NOR and τ coefficients are also tuned and adjusted under an external applied transverse electric (F) and magnetic (B) fields.

This paper is organized as follows: In section 2, the 3D Schrödinger equation is given in the effective mass approximation. Due to the geometrical complexity, we have adopted the numerical method of Finite Difference Method (FDM) to solve the 3D Schrödinger equation. Section 3, is preserved to discuss and to perform the obtained results, where the structural dimensions, the wetting layer, the hydrostatic pressure, the temperature and the electromagnetic fields effects are introduced together. Finally, a conclusion and some perspectives are presented in the last section.

Theoretical framework

By using the molecular beam epitaxy (MBE) technology, InAs material is deposited on (001) GaAs wafer. When the active material (InAs) reaches ~ 0.5 nm, so called the wetting layer (WL), InAs QD with lens-shaped will be formed. Here, the QD with radius R_1 in (xoy) plane and height h_1 in (001) growth play the role of the core. Next, the core is cupped with the GaAs shell material with thickness R_2-R_1 and height h_2-h_1 in (xoy) plane and (001) direction, respectively. Figure 1 shows a schematic cross-section of the nanostructure under investigation. In this work, R_i and h_i (i=1, 2) will be used as tuning parameters.

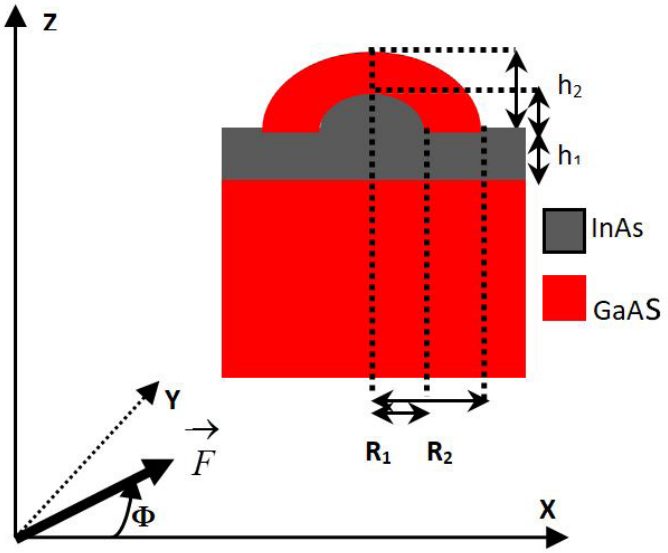

Figure 1: Schematic cross-section along y-axis of the cor/shell strucure.

In the framework of effective- mass approximation, the electron energy eigenvalues (E) and the envelope functions ($\psi(\vec{r})$) of a single confined electron in such nanostructure are given by the following 3D Schrödinger equation [22, 23]:

$$-\frac{h^2}{8\pi^2}\left[\vec{\nabla}.(\frac{1}{m^*(\vec{r},P,T)}\vec{\nabla})+V(\vec{r},P,T)\right]\psi(\vec{r})=E\psi(\vec{r}) \quad (1)$$

Where h is the Planck's constant and $\vec{r}=(x,y,z)$ is the electron vector position, respectively. Also, in this work, we have introduced the hydrostatic pressure and temperature effects via the electron- effective mass $m*$ and the energy gap E_g^{Γ}. So, the conduction band electron effective- mass for the Γ valley is given by [24]:

$$\frac{m_0}{m^*(\vec{r},P,T)}=1+2\gamma+\left[\frac{E_P^{\Gamma}(E_g^{\Gamma}+\frac{2}{3}\Delta_{S0})}{E_g^{\Gamma}(E_g^{\Gamma}+\Delta_{S0})}\right] \quad (2)$$

Where γ is the Kane variable, m_0 is the free electron mass, E_p^{Γ} is the energy related to the momentum matrix element, Δ_{S0} is the spin-orbit splitting, and E_g^{Γ} is the energy gap which is temperature (T) and pressure (P) dependent quantity given by [25]:

$$E_g^{\Gamma}(P,T)=E_g^{\Gamma}(0,0)-\frac{\alpha T^2}{\beta+T}+D.P \quad (3)$$

The recommended and adopted parameters used in Eqs. (2 and 3) are summarized and listed in Refs [24, 25].

Accordingly, the 3D dimensional confining potential under pressure and temperature effects is given by:

$$V(\vec{r},P,T)=\begin{cases}0, & \text{inside InAs shell } and \text{ } WL\\ Q_c\left[E_g^{\Gamma}(GaAs)-E_g^{\Gamma}(InAs)\right], & inside \text{ } core\\ \infty, & \text{elsewhere}\end{cases} \quad (4)$$

Where, the conduction band offset between GaAs and InAs materials is assumed to be $Q_C=70\%$ [25].

Due to the geometrical complexity of the structure under investigation, we have adopted the Finite Difference Method (FDM) to solve the 3D Schrödinger equation (Eq.1). So, in this work, the structure under simulation (Fig.1) is discretized into $N_x = N_y = N_z = 128$ nodes with a mesh size Δ = 3.17 Å ($L_x = L_y = L_z = 40$ nm) along x, y and z directions, respectively. At each grid point ($(x_i, y_j, z_k) = (i, j, k)$, where i, j and k =1, 2, ... N_z), we will symbolize the wave function by ψ(i, j, k). Then, the first spatial derivative will be approximate by the central finite difference scheme given by means of a Taylor expansion with the truncation error $O\left(\left[\frac{\Delta}{2}\right]^2\right)$ as shown below:

$$\begin{aligned}\frac{\partial\psi(i,j,k)}{\partial x}&=\frac{\psi(i+1,j,k)-\psi(i-1,j,k)}{2\Delta}+O\left(\left[\frac{\Delta}{2}\right]^2\right)\\ \frac{\partial\psi(i,j,k)}{\partial y}&=\frac{\psi(i,j+1,k)-\psi(i,j-1,k)}{2\Delta}+O\left(\left[\frac{\Delta}{2}\right]^2\right)\\ \frac{\partial\psi(i,j,k)}{\partial z}&=\frac{\psi(i,j,k+1)-\psi(i,j,k-1)}{2\Delta}+O\left(\left[\frac{\Delta}{2}\right]^2\right)\end{aligned} \quad (5)$$

By using the standard boundary conditions:

$$\psi(i,j,k)\to 0 \quad as \quad i,j,k\pm\infty \quad (6)$$

It remains $(N_z\text{-}2)^3$ linear equations will be solved. So, the finite difference representation of the Schrödinger equation given by Eq.(1) can be rearranged as:

$$\begin{aligned}&A(i,j,k)\psi(i,j,k)+B(i,j+1,k)\psi(i,j+1,k)+C(i+1,j,k)\psi(i+1,j,k)\\&+D(i,j-1,k)\psi(i,j-1,k)+E(i-1,j,k)\psi(i-1,j,k)\\&+F(i,j,k+1)\psi(i,j,k+1)+G(i,j,k-1)\psi(i,j,k-1)=E\psi(i,j,k)\end{aligned} \quad (7)$$

Where

$$\begin{aligned}A(i,j,k)&=\frac{\hbar^2}{4\Delta^2}\left\{\begin{matrix}\frac{6}{m^*(i,j,k)}+\frac{1}{m^*(i-1,j,k)}+\frac{1}{m^*(i+1,j,k)}\\+\frac{1}{m^*(i,j-1,k)}+\frac{1}{m^*(i,j+1,k)}\\\frac{1}{m^*(i,j,k-1)}+\frac{1}{m^*(i,j,k+1)}\end{matrix}\right\}+V(i,j,k)\\ B(i,j+1,k)&=\frac{-\hbar^2}{4\Delta^2}\left\{\frac{1}{m^*(i,j,k)}+\frac{1}{m^*(i,j+1,k)}\right\}\\ C(i+1,j,k)&=\frac{-\hbar^2}{4\Delta^2}\left\{\frac{1}{m^*(i,j,k)}+\frac{1}{m^*(i+1,j,k)}\right\}\\ D(i,j-1,k)&=\frac{-\hbar^2}{4\Delta^2}\left\{\frac{1}{m^*(i,j,k)}+\frac{1}{m^*(i,j-1,k)}\right\}\\ E(i-1,j,k)&=\frac{-\hbar^2}{4\Delta^2}\left\{\frac{1}{m^*(i,j,k)}+\frac{1}{m^*(i-1,j,k)}\right\}\\ F(i,j,k+1)&=\frac{-\hbar^2}{4\Delta^2}\left\{\frac{1}{m^*(i,j,k)}+\frac{1}{m^*(i,j,k+1)}\right\}\\ G(i,j,k-1)&=\frac{-\hbar^2}{4\Delta^2}\left\{\frac{1}{m^*(i,j,k)}+\frac{1}{m^*(i,j,k-1)}\right\}\end{aligned} \quad (8)$$

Therefore, resolution of the Eqs.(7) system gives access to the eigen energies (E_i) and their corresponding envelope functions ($\psi_i(x,y,z)$). For more details to use this numerical

method, researchers are referred to [26]. So, after the eigen energies and their corresponding envelope wave functions are obtained, the Nonlinear Optical Rectification (NOR) can be calculated within the framework of the density-matrix formalism. So, under an incident electromagnetic field with frequency ω:

$$E(t) = \tilde{E}_0 e^{i\omega t} + \tilde{E}_0 e^{-i\omega t} \tag{9}$$

an electronic polarization of the system is generated:

$$P(t) = \varepsilon_0 \chi^{(1)}(\omega)\tilde{E}_0 e^{i\omega t} + \varepsilon_0 \chi^{(2)}_{2\omega}(2\omega)\tilde{E}_0^2 e^{2i\omega t} + \varepsilon_0 \chi^{(3)}_{3\omega}(3\omega)\tilde{E}_0^3 e^{3i\omega t} + cc + \varepsilon_0 \chi_0^{(2)} \left|\tilde{E}_0\right|^2 \tag{10}$$

Terms $\chi^{(1)}, \chi^{(2)}_{2\omega}(2\omega), \chi^{(3)}_{3\omega}(3\omega)$ are the linear, the second and the third order nonlinear optical susceptibilities, respectively.

Based on the density matrix approach, the NOR coefficient is given by [25]:

$$\chi_0^{(2)} = \frac{4N\mu_{12}^2\delta_{21}}{\varepsilon_0} \frac{E_{21}^2\left[1+\frac{\Gamma_2}{\Gamma_1}\right] + \left[(\omega)^2 + (\Gamma_2)^2\right]\left[\frac{\Gamma_2}{\Gamma_1} - 1\right]}{\left[(E_{21} - \hbar\omega)^2 + (\Gamma_2\hbar)^2\right]\left[(\xi_{21} + \hbar\omega)^2 + (\Gamma_2)^2\right]} \tag{11}$$

where $N = 3\ 10^{22} m^{-3}$ is the volume density of carriers in the system, $\delta_{21} = \left|\mu_{22} - \mu_{11}\right|$, where $\mu_{ij} = \langle \psi_i | er | \psi_j \rangle$ is the dipole matrix element, $E_{21} = E_2 - E_1$ is the transition energy between the ground and first excited states, $\Gamma_1 = \frac{1}{T_1} = 1\ ps^{-1}$ and $\Gamma_2 = \frac{1}{T_2} = 5\ ps^{-1}$ $\Gamma_2 = \frac{1}{T_2}$ are the diagonal and the off-diagonal relaxation rates, respectively and $\hbar\omega$ is the incident photon energy.

Also, in this paper we have investigated the combined effects of pressure, temperature and electromagnetic fields on the transition lifetime of carriers between the ground and the first excited states given by [26]:

$$\tau = \frac{3c^3\hbar^4\pi\varepsilon_0}{E_{21}^3 n_r \left|\mu_{12}\right|^2} \tag{12}$$

Where ε_0 is the vacuum permittivity, C is the speed of light and $n_r = 3{,}2$ is the refractive index.

Results and Discussions

We compute numerically the NOR coefficient under the influence of hydrostatic pressure, temperature and electromagnetic fields. To start, our calculations are performed for P = 0, T =300 K, F = 0 and B = 0. Figure 2 shows the variation of the NOR coefficient as a function of the incident photon energy for different configurations of the structure understudy.

Compared to a semi-spherical core/shell system ((c): $h_1 = R_1 = 5$ nm and $h_2 = R_2 = 8$ nm), NOR intensity is the lower and a red-shift is obtained with a lens-shaped structures ((a) and (b) spectra). This shift is due to a decrease of the energy difference (E_2 - E_1) between the lower and upper states with increasing the core radius (R_1). Also, note that the NOR magnitude decreases as the core radius increases. This behavior is due to a decreasing of the geometrical factor ($\mu_{12}^2\delta_{21}$) with R_1 as indicated explicitly from Eq.(11).

To better understand the core radius effect on the NOR magnitude and on the corresponding resonant energy (ω_{res}), in **Figure 3**, we have plotted the first lowest energy (E_1 and E_2) states and the resonant energy (ω_{res}) of the NOR coefficient as a function of the core radius for the configuration (a) of Figure 2 as a reference structure.

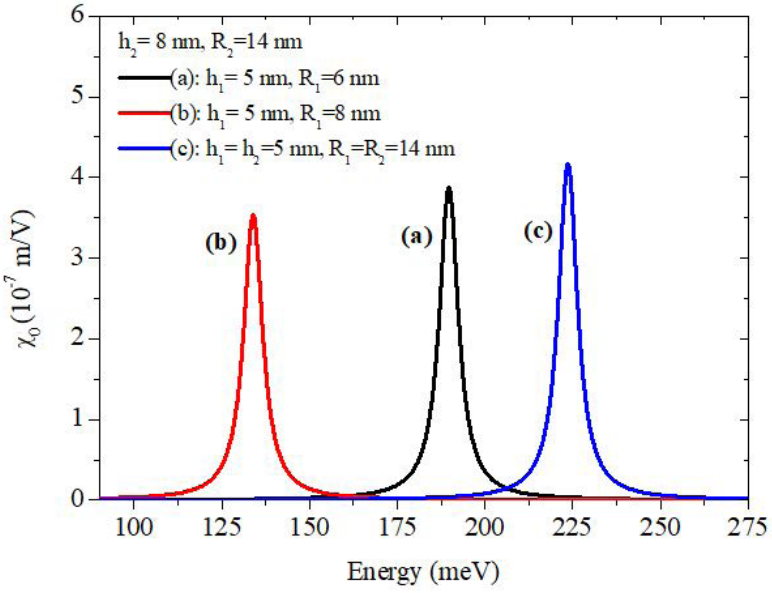

Figure 2: NOR versus incident photon energy for different core radius

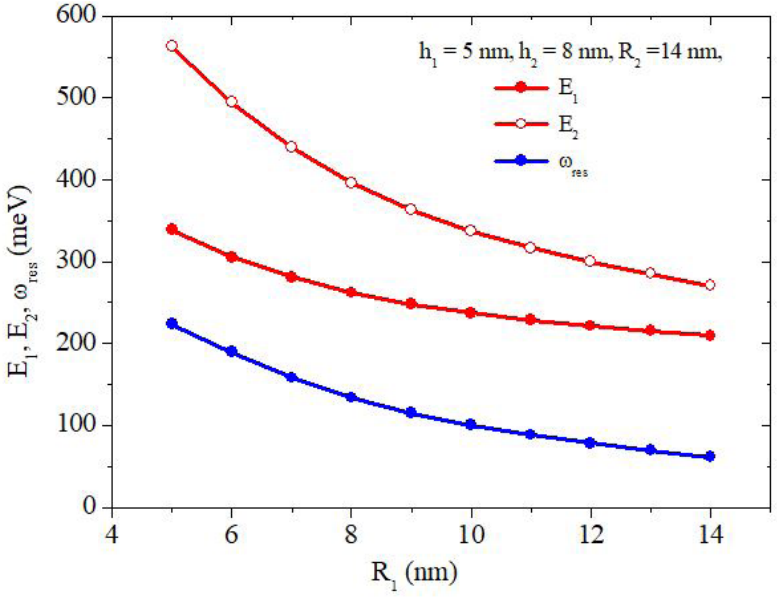

Figure 3: Energies eigen values of the ground and first excited states and the resonant energy ω_{res} as a function of the core radius

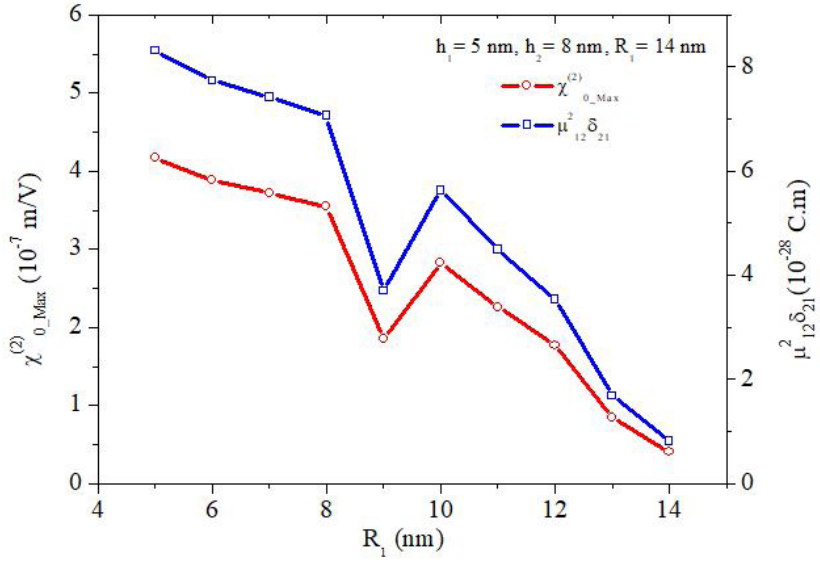

Figure 4: NOR magnitude (left) and the geometrical factor (right) as a function of the core radius

It is clearly seen, that E_1 and E_2 decreases with increasing the core radius, so, the shell width (R_2-R_1) decreases and a red- shift of the NOR peak is obtained, ω_{res} decreases. This shift is attributed to the reduction of the confinement of carriers after increasing the core width. Therefore, the core radius can be used as a tuning parameter to adjust the NOR peak position.

The decrease (or increase) in NOR magnitude can be clearly explained by comparing the NOR magnitude ($\chi^{(2)}_{0\_Max}$) and the geometrical factor as function of the core radius, as depicted in Figure 4.

It is clearly seen that the NOR magnitude is directly proportional to the geometrical factor ($\mu^2_{12}\delta_{21}$) which is not a monotonic function of the core radius. Thus, the decrease in the quantity $\mu^2_{12}\delta_{21}$ as the core radius increased is attributed to a lower degree of overlap among the envelope wave functions of the ground and first excited states. So, the maximum value of the NOR coefficient is obtained for a lower (higher) core (shell) radius. Also, in the experimentally side, it is found that under the capping layer, the QD height decreases. Therefore, in this work and for the all remaining simulations, we have assumed the lens-shaped of the core/shell structure as the realistic model of the QD shape.

As mentioned above, the electron's localization is affected by the quantum dot morphology. So, to better understand the wetting layer, core and shell thickness on confinement effect, we present the probability of finding an electron in the core region (P_C), shell material (P_S) and wetting layer (P_{WL}) for the ground (Figure 5(a)) and first excited (Figure 5(b)) states as a function of the core radius. The probability of finding and electron in each material is given by:

$$\frac{\int_{C/WL,S}|\psi_i|^2 d^3r}{\int_{system}|\psi_i|^2 d^3r}\times 100 \qquad (13)$$

Obtained results show that the wetting layer effect is more pronounced for a smaller core thickness (R_1< 8 nm). So, the probability of finding an electron inside the wetting layer decreases with increasing the core radius. As well, as we can see in Figure 5(a), the electron is confined inside the core material with a probability P_C = 81%, which increases with increasing (decreasing) the core (shell) radius. However, the probability of finding an electron confined inside the shell region is less than P_S= 1%. Also, for the first excited state (Fig.5(b), we can see that the probability of finding an electron in the core region increases from P_C= 67.5% to 82.5% with increasing the core radius from 5 to 14 nm. However, the probability of finding an electron inside the wetting layer decreases from P_{WL}=14% to 11% as the core radius increases and P_S doesn't exceed 1%. Thus, the shell radius (R_2-R_1) decreases as the core radius (R_1) increases and the electronic wave function confined in the shell region moved from the wetting layer and the barrier material (GaAs) toward the core region. Thus, the unavoidable effects of the wetting layer on the energy eigen values, consequently on the NOR magnitude and on the transition energy (ω_{res}), are of great importance. To better understand the wetting layer and core size effects, Figure 6 shows the NOR coefficient versus the incident photon energy with and without the wetting layer and for two different values of the core height.

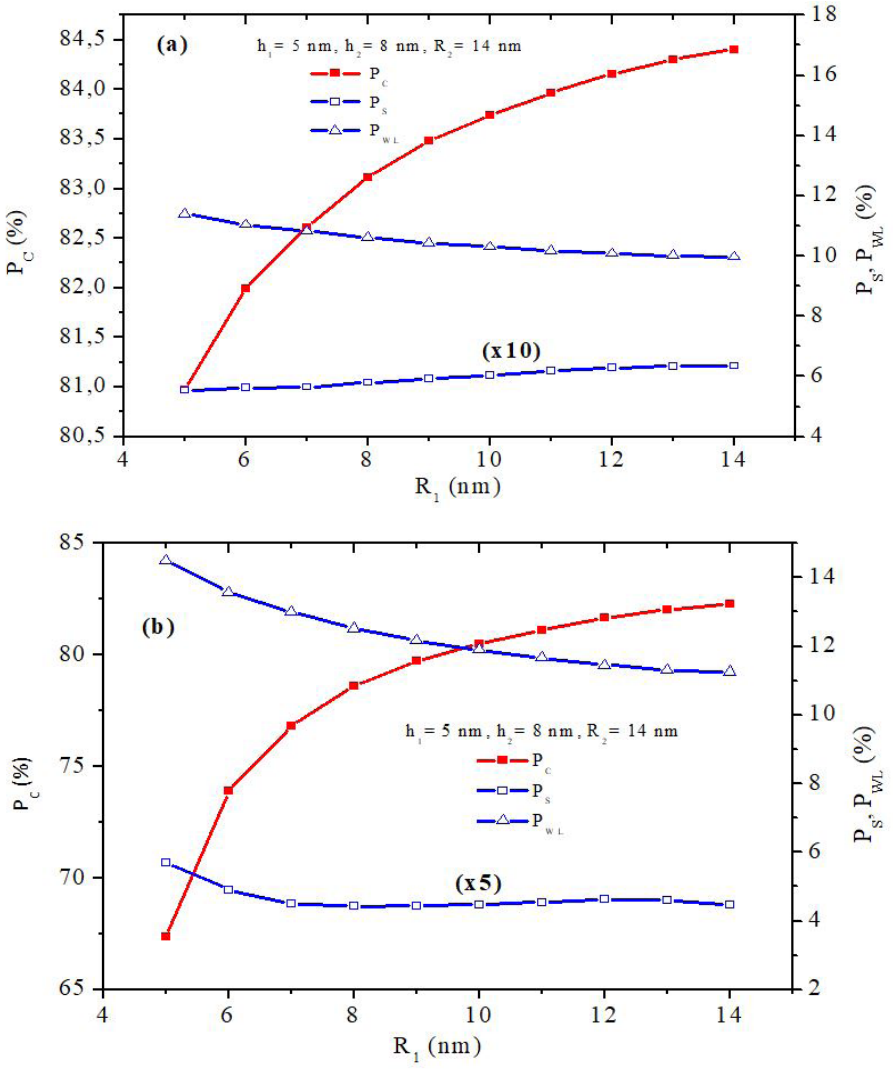

Figure 5: Probability of finding electron inside the core region (P_C), the shell region (P_S), and in the wetting layer (P_{WL}) as a function of the core radius for: (a) the ground energy level and (b) the first excited energy level

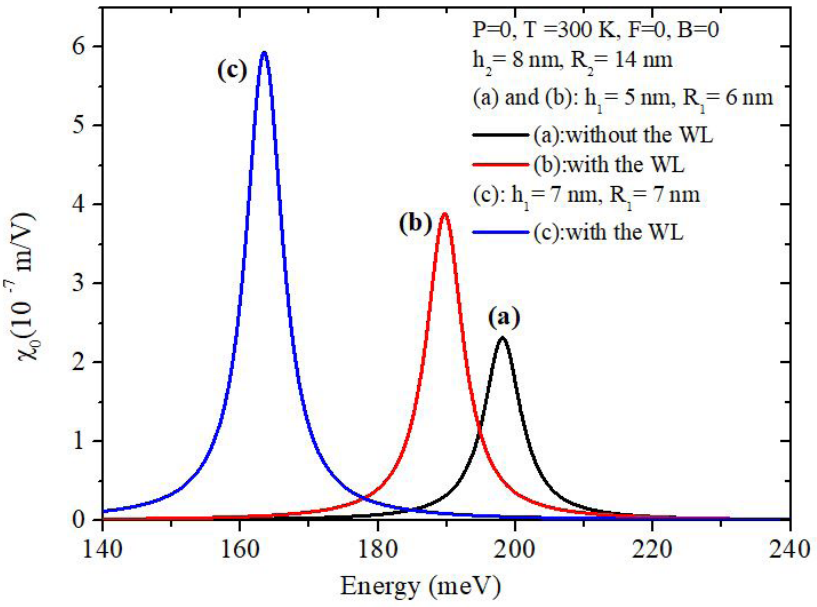

Figure 6: NOR coefficient versus the incident photon energy with and without the wetting layer and for two different values of the core height

Compared with the spectrum (a), it is clearly seen, that the NOR spectrum displays a red-shift by about 9 meV with considering the wetting layer effects (spectrum b) and the NOR magnitude increases by about 65%. So, obtained results show that the unavoidable effect of the WL on the electronic and optical properties of semiconductor QDs systems is of significant importance. As well, the NOR coefficient experiences a red-shift and increases in magnitude with increasing the quantum core height (b and c spectra). These behaviors are essentially explained by the reduction of the confinement of carriers and the increase of the geometrical factor after increasing the quantum core height.

Now, we search to adjust and optimize the NOR coefficient under an applied transverse electric field given by (see Figure.1):

$$\vec{F} = F(\cos(\phi)\vec{e}_x + \sin(\phi)\vec{e}_y) \tag{14}$$

So, we have assumed this structure configuration (h_1 = 5 nm, R_1=6 nm, h_2= 8 nm and R_2 = 14 nm) as a reference system, and we have set pressure, temperature and magnetic field intensity to zero, 300 K and zero, respectively. The electric field intensity effect on the NOR coefficient is then investigated as depicted in Figure 7.

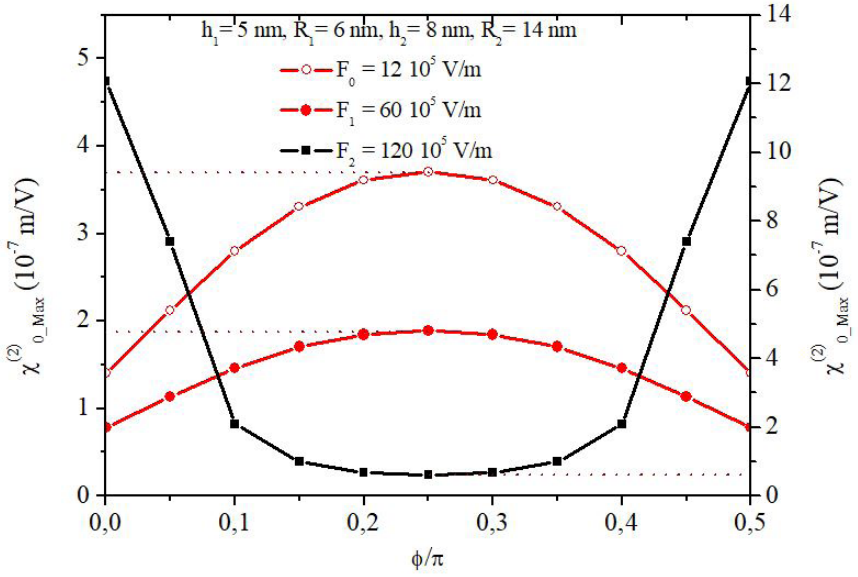

Figure 7: NOR magnitude versus the angle Φ for different electric field intenisties

This figure shows the NOR magnitude versus the angle Φ for different electric field intensities. It reveals that the optimized NOR coefficient ($\chi^{(2)}_{0\_Max} = 12\ \ 10^{-7} m/V$)) is obtained with an intense electric field (F = 12 10^5 V/m) applied along the x-axis (Φ = 0) or y-axis (Φ = π/2) of the structure under investigation. To better understand the electric field intensity (F) effect on the NOR coefficient, we have plotted the variation of the NOR magnitude and the geometrical factor as a function of the electric field intensity, as shown in Figure 8.

As we can see, the NOR magnitude is directly proportional to the geometrical factor, which is not a monotonic function of the electric field intensity. Moreover, at lower electric field intensity, NOR magnitude decreases with increasing the electric field intensity and tend to zero for a specific value of the electric field intensity, F_C= 80 10^5 V/m. This phenomenon is attributed to the symmetry of the wave functions in the system under study. At this quenching electric field intensity, the wave functions in the structure understudy become either symmetric or anti-symmetric, which makes the dipole matrix elements μ_{11} and μ_{22} to become null, and so the electron displacement δ_{21}= μ_{22} - μ_{11} as well. Thus, as deduced from Figures 7 and 8, the designed core/shell structure can be used under high intense electric field oriented along one side of the cross-section (xoy), along x-axis (Φ = 0) or y-axis (Φ = π/2). Here, the NOR coefficient reaches the 12 10^{-7} m/V magnitude at F =120 10^5V/m.

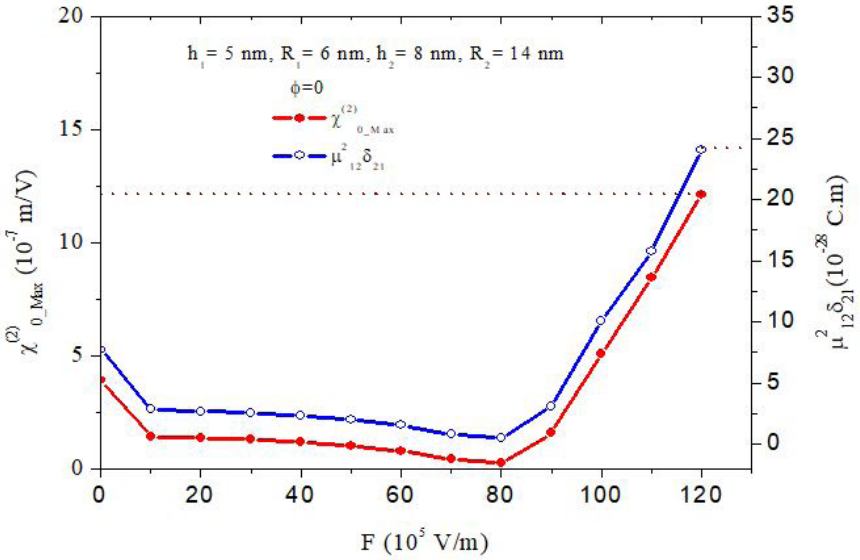

Figure 8: NOR magnitude (left axis) and the geometrical factor (right axis) versus the electric field intensity for Φ=0)

In the same means, obtained results also show that the electric field intensity influences both the lowest energy states and the NOR resonant energy, as depicted in Figure 9.

It is clearly seen, at lower electric field intensity (F < 80 10^5 V/m), the resonant energy of the NOR coefficient remains constant. Nevertheless, at higher electric field intensity, the Stark effect is noticeably and the resonant energy ω_{res} decreases with increasing the electric field intensity.

Taken in the above simulations, to more show the dependence of the NOR coefficient on the electric field intensity and orientation, the nonlinear optical rectification curves versus the incident photon energy for two values of F and φ are given by Figure 10.

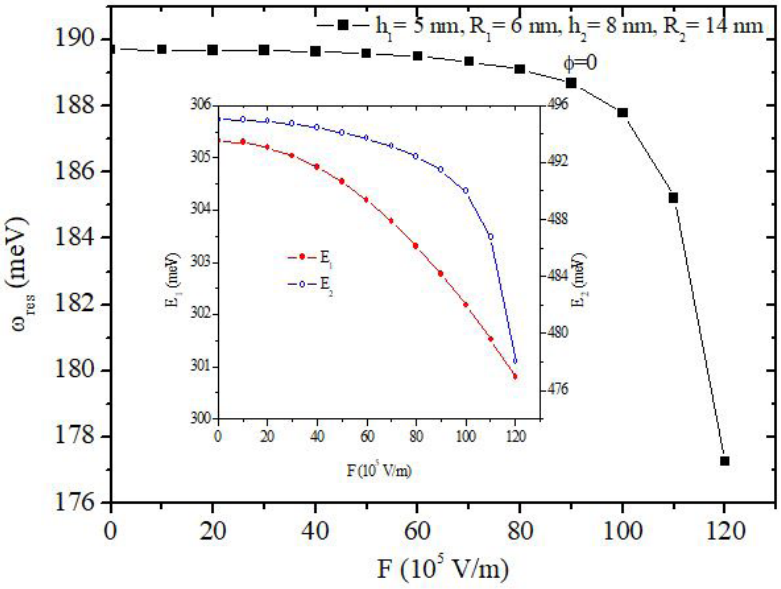

Figure 9: The resonant energy versus the electric field intensity for Φ=0 (energies eigen values of the ground and first excited states are depicted by the sketched figure)

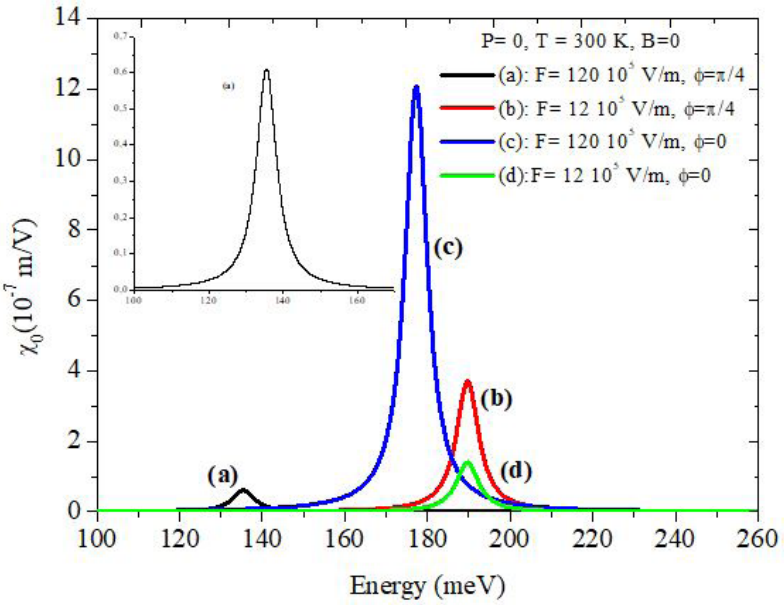

Figure 10: The NOR as a function of the incident photon energy for different electric field intensities and orionatations (the sketched figure is a zoom of the spectrum (a)

In agreement with the previous results, it is clear seen that the maximum value of the NOR coefficient ($\chi^{(2)}_{0\_Max} = 12\ \ 10^{-7} m/V$) is obtained at higher electric field intensity (F = 120 10^5 V/m) applied along the x-axis (φ=0), (a) and (c) spectra. However, at lower electric field intensity (F = 12 10^5 V/m), the NOR coefficient reaches its maximum $\chi^{(2)}_{0\_Max} = 3.8\ \ 10^{-7} m/V$, where the electric field is oriented along the diagonal (Φ = π/4) of the crsos section (xoy) of the structure under investigation, (b) and (d) spectra.

In summary, obtained results are very important and show that the quantum core/shell dimensions, the electric field intensity and orientation can be used as tuning parameters to optimize the NOR coefficient with adjusted magnitude and resonant energy.

During simulation, we have also found that the magnetic field intensity, pressure and temperature can also affect the asymmetry of the core/shell structure under investigation and then the NOR coefficient. So, combined effects of the above-mentioned proofs on the NOR spectra are illustrated by Figure 11.

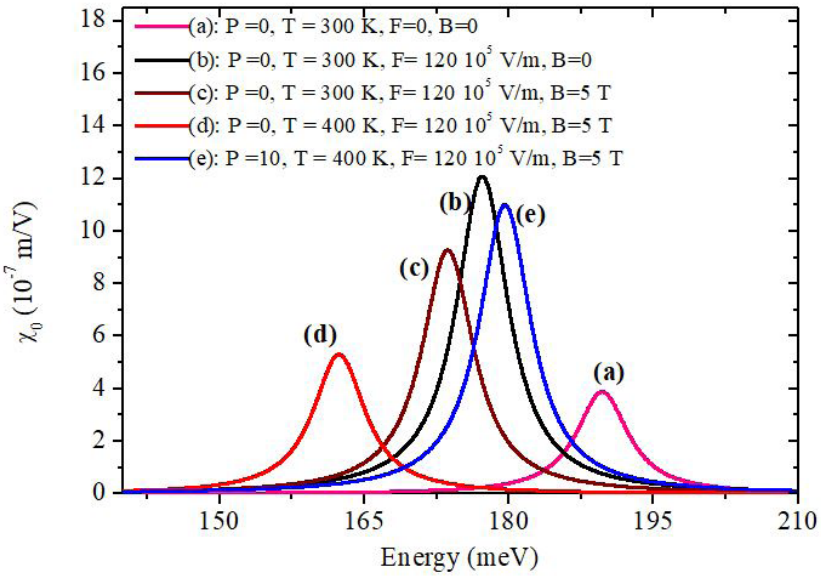

Figure 11: Combined effects of pressure, temperature, electromagnetic fields and wetting layer on the NOR spectrum

Here, obtained results are presented under an intense electric field (F = 120 10^5 V/m) applied along the x-axis (Φ = 0). We note that the NOR coefficient decreases in magnitude and experiences a red-shift with increasing the magnetic field intensity, (b) and (c) spectra. This is attributed to a change of the geometrical factor and the confining potential with the magnetic field intensity. So, it is clear seen, that the magnetic field effect can also be used as a tuning parameter to control the NOR spectrum. It also can be seen that the NOR peak displays a blue- shift with increasing the hydrostatic pressure, (d) and (e) spectra. This is due to an increasing of the confining potential, followed by an increasing of the separation energy between the ground and first excited energies (E_2-E_1). Also, an increasing of the hydrostatic pressure increases the electron effective- mass of the electrons. Moreover, with increasing the pressure, the NOR magnitude increases and reaches $\chi^{(2)}_{0\_Max} = 11\ \ 10^{-7} m/V$ m/V value. This is related to the increasing of the geometrical factor with pressure. We note that the pressure related changes are mainly due to the pressure dependence of the energy gap of both GaAs and InAs materials, as indicated from Eq.(3). Nevertheless, a red-shift is achieved with increasing the temperature, (c) and (d) spectra.

This is explained by the reduction of the confining potential and to a decreasing of the electron effective- mass with increasing the temperature. So, the opposite effects caused by pressure and temperature reveal a big practical interest and offer an alternative way to tuning of the nonlinear optical properties in lens- shaped core/shell structure coupled to its wetting layer in optoelectronic devices.

According to obtained results, we show that the NOR coefficient is influenced by the temperature, the pressure and the electromagnetic fields intensities. So, these proofs cause a change of the dipole matrix element $\mu_{12} = \langle \psi_1 | er | \psi_2 \rangle$ and the transition energy $E_{21} = E_2 - E_1$, accordingly, the transition lifetime (τ) of carriers is also affected. So, at this step, we take advantage to investigate and analyze the pressure, temperature and the electromagnetic fields effects on the transition lifetime. Hence, Figure 12 illustrates the transition lifetime between the ground and the first excited states as a function of the temperature and for different values of P, F and B.

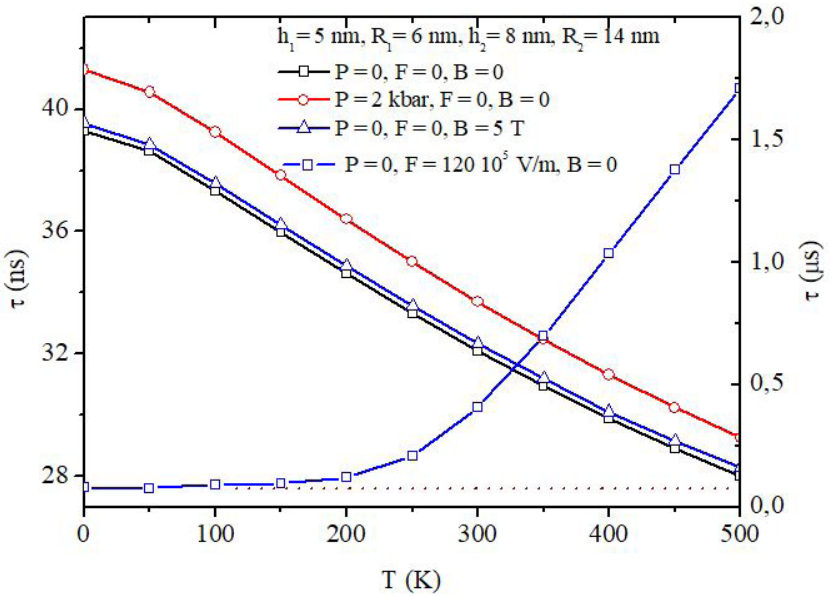

Figure 12: Pressure, temperature and electromagnetic fields effects on the transition lifetime of carriers

It is clearly seen, that τ decreases from 39 to 28 ns according to a quadratic function as the temperature increases from 0 to 500 K. Thus, the increase in temperature leads to a reduction of the confining potential and the effective- mass of carriers. Therefore, at a fixed pressure, F and B intensities, the transition energy (E_{21}) displays a red-shift and the product $E_{21}^3\left|\mu_{12}\right|^2$ (see Eq.12) increases as the temperature increases, so, the intra-band transition lifetime decreases. However, the reverse behavior is obtained with increasing the pressure. Consequently, the transition lifetime behavior of τ with T and P is attributed to the matched behaviors of the transition dipole matrix element and the transition energy with increasing the temperature or pressure. As well, the increase of the magnetic field intensity (B) leads to a change of the confining potential geometry and reduces the electron confinement effects. So, increasing B leads to increasing the probability of penetration of the wave functions into the core material. As a result, the transition dipole moment increases while the transition energy decreases. Consequently, the transition lifetime which is inversely proportional to the product $E_{21}^3\left|\mu_{12}\right|^2$ displays a slight increase with the magnetic field intensity. However, in the range 0 - 200 K, the intra-band transition lifetime of carriers remains constant with increasing the electric field intensity (left axis) and then increases significantly from 80 nm to 1.7 μs. Accordingly, the non-monotonic behavior of τ with the electric field intensity and temperature is attributed to the concurrent behaviors of the transition dipole moment element (μ_{12}) and the transition energy E_{21} with T and F as depicted in Figure 13.

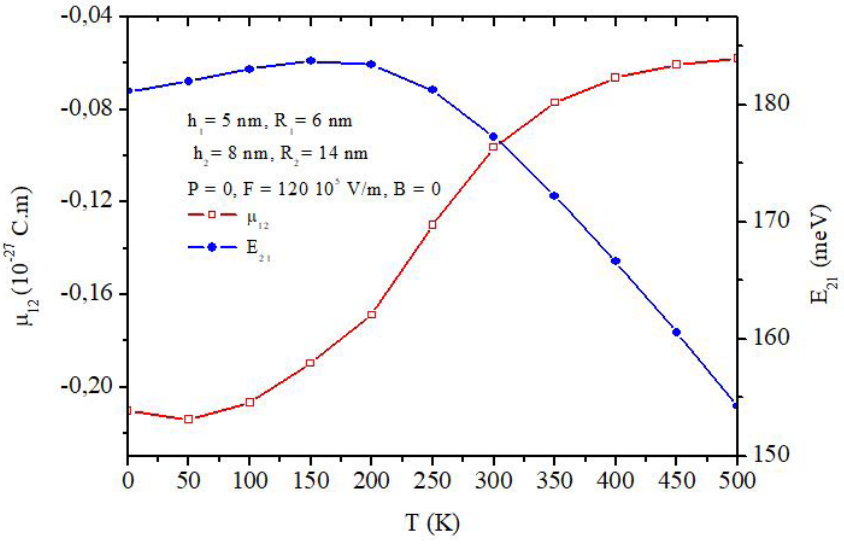

Figure 13: Temperature and electric field intensity effects on the transition dipole matrix element (left axis) and on the transition energy (right axis)

To summarize, obtained results are important and helpful for researchers to design a lens-shaped core/shell nanostructures based on the NOR coefficient with adjusted and optimized magnitude. Therefore, structure dimensions, hydrostatic pressure, temperature and electromagnetic fields can be used as tuning parameters and gives a new degree of freedom to achieve a large NOR with adjusted resonant energy, magnitude and intra-band transition lifetime of carriers. So, by passing an intense laser beam, the designed core/shell structure can be used as a rectifier to turn a sinusoidal electric field into a direct current polarization, as indicated from Eq.10. As well, in the near future researcher works, the ultrafast response time of the NOR make it a good candidate for the development of solar cells so-called rectenna device. In such device, the NOR will be combined with optical nanoantenna to built an efficient solar energy converter. Consequently, our study constitutes a good theoretical support for researchers in order to achieve these objectives.

Conclusion

With the framework of the density matrix formalism, the nonlinear optical rectification and the intra- band transition lifetime in a single lens-shaped core/shell are well investigated. Calculations are performed by using the FDM method of second order. All parameter effects such as: the wetting layer, the hydrostatic pressure, temperature and electromagnetic fields are introduced together. It is found that the NOR coefficient experiences a red or a blue- shift, as well, the intra-band transition lifetime increases or decreases by tuning the proofs mentioned above. So, the NOR spectrum displays a red-shifted by about 9 meV with considering the wetting layer effect. Also, obtained results indicate that the NOR coefficient displays a red- shift with increasing the core radius or height. As well, the opposite effects caused by hydrostatic pressure and temperature reveal a big practical interest and offer an alternative way to tuning of the NOR in optoelectronic devices. In addition, it is found that the designed core/shell structure can be used under intense electric field applied along one side ($\Phi = 0$ or $\Phi = \pi/2$) of the cross-section (xoy) of the structure under study. Therefore, all the mentioned proofs can be used as tuning parameters to achieve a large NOR coefficient with adjusted resonant energy and intra-band transition lifetime of carriers.

During simulations, we have also found that the nanostructure under investigation confines more than two level states. So, this behavior gives opportunity to investigate other nonlinear optical properties such as: the Second (SHG) and the Third Harmonic (THG) Generations. This work will be also adopted to explore the nonlinear optical properties in coupled quantum core/shell in future investigations.

References

1. Alves FDP, G Karunasiri, N Hanson, M Byloos, HC Liu, et al. (2007) "T NIR, MWIR and LWIR quantum well infrared photodetector using interband and intersubband transitions," Infrared Phys Technol 50: 182-6.

2. TC Newell, DJ Bossert, A Stintz, B Fuchs, KL Malloy (1999) "Gain and line width enhancement factor in InAs quantum-dot laser diodes," IEEE J. Quantum Electron 11: 1527-9.

3. U Aeberhard, RH Morf (2008) "Microscopic non equilibrium theory of quantum well solar cells". Phys Rev 77: 125343.

4. JX Chen (2002) Tuning InAs/GaAs quantum dot properties under Stranski-Krastanov growth mode for 1.3 μm applications. J Appl Phys 91: 6710.

5. M Cusack, P Briddon, Ma Jaros (1996) Electronic structure of InAs/GaAs self-assembled quantum dots," Physical Review B 54: 2300.

6. M Royo, JI Climente, J Planelles (2011) Emission spectrum of quasi resonant laterally coupled quantum dots. Phys Rev B 84: 235312.

7. Wenfang Xie (2013) The nonlinear optical rectification coefficient of quantu dots and rings with a repulsive scattering center. J Luminescence 143: 27-30.

8. Zaiping Zeng, Christos S, Garoufalis, Sotirios Bascoutas (2014) Linear and nonlinear optical susceptibilities in lateral coupled quantum- dot- quantum- ring system. Physics Letters A 378: 2713-8.

9. M Sabaeian, A Khaledi-Nasab (2012) Size-dependent intersubband optical properties of dome-shaped InAs/GaAs quantum dots with wetting layer. Applied Optics 51: 4176.

10. M Paul, P Bhattacharya, B Das, S Rani (2011) Dependence of second order nonlinear susceptibility and efficiency on shape of CdS quantum dot," Journal of Electrical and Electronics Engineering Research 3: 134-42.

11. G Rezaei, M Vahdani, B Vaseghi (2011) Nonlinear optical properties of a hydrogenic impurity in an ellipsoidal finite potential quantum dot. Current Applied Physics 11: 176.

12. M Shahzadeh, M Sabaeian (2015) Numerical analysis of optical properties of oblate semi-spheroid-shaped quantum dots coupled to wetting layer. J Optical Society of America B 32: 1097.

13. Gh Safarpour, M Barati (2013) The optical absorption coefficient and refractive index changes of a spherical quantum dot placed at the center of a cylindrical nano-wire," J Luminescence 137: 98-104.

14. B Liang, P Wong, N Pavarelli, J Tatebayashi, T Ochalski, G Huyet, et al. (2011) Lateral interdot carrier transfer in an InAs quantum dot cluster grown on a pyramidal GaAs surface. Nanotechnology 22: 055706.

15. JX Chen (2002) Tuning InAs/GaAs quantum dot properties under Stranski-Krastanov growth mode for 1.3 μm applications. J Appl Phys 91: 6710.

16. L Bouzaïene, L Sfaxi, M Baira, H Maaref, C Bru-Chevallier (2011) Power density and temperature dependent multi-excited states in InAs/GaAs quantum dots. J Nanopart Res 13: 257-62.

17. EC Niculescu, M Cristea, A Spandonide (2013) Exciton states in CdSe/ZnS core–shell quantum dots under applied electric fields. Superlattices and Microstructures 63: 1–9.

18. M ElHaouari, ATalbi (2017) Linear and nonlinear optical properties of a single dopant in strained AlAs/GaAs spherical core/shell quantum dots. Optics Communications 383: 231–7.

19. Mohammad Kouhi (2017) Study of nonlinear optical absorption in GaN/AlGaN core–shell nanowire," J Nanophoton 11: 016012.

20. Hatice Taş, Mehmet Şahin (2012) The electronic properties of a core/shell/well/shell spherical quantum dot with and without a hydrogenic impurity. J Appl Phys 111: 083702.

21. M Cristea, A Radu n, EC Niculescu (2013) Electric field effect on the third-order non linear optical susceptibility in inverted ore–shell nanodots with dielectric confinement," J Luminescence: 143592–9.

22. Varsha Mohamed Kria (2021) Quantum Confined Stark Effect on the Linear and Nonlinear Optical Properties of SiGe/Si Semi Oblate and Prolate Quantum Dots Grown in Si Wetting Layer," Nanomaterials 11: 1513.

23. Shuai Shao, Kang-Xian Guo (2011) Studies on the second-harmonic generations in cubical quantum dots with applied electric field. Physica B 406: 393-6.

24. I Vurgaftman, JR Meyer, LR Ram-Mohan (2001) Band parameters for III–V compound semiconductors and their alloys," J Appl Phys 89: 5818-27.

25. Gh Safarpour, M Moradi, M Barati (2012) Hydrostatic pressure and temperature effects on the electronic energy levels of a spherical quantum dot placed atthe center of a nano-wire, "Superlattices Microstruct 52: 687-96.

26. M Choubani, D Makhlouf, F Saidi, H Maaref (2020) Enhancement of the second harmonic generation in a coupled lens-shaped quantum dots under wetting layer, temperature, pressure, and electric field effects. Optical and Quantum Electronics 52: 1-15.

27. I Karabulut, ME Mora-Ramos, CA Duque (2011) Nonlinear optical rectification and optical absorption in asymmetric double quantum wells: Combined effects of applied electric and magnetic fields and hydrostatic. J Luminescence 131: 1502-9.

28. A Yariv (1989) Quantum electronics 3rd," Edn. (John-Wiely & Sons, New York, 1988): 389.